

Electron Spin Resonance of $\text{SrCu}_2(\text{BO}_3)_2$ at High Magnetic FieldS. El Shawish,¹ J. Bonca,^{1,2} C. D. Batista,³ and I. Sega¹¹J. Stefan Institute, SI-1000 Ljubljana, Slovenia²Faculty of Mathematics and Physics, University of Ljubljana, SI-1000 Ljubljana, Slovenia³Theoretical Division, Los Alamos National Laboratory, Los Alamos, NM 87545, USA

(Dated: 22nd March 2024)

We calculate the electron spin resonance (ESR) spectra of the quasi-two-dimensional dimer spin liquid $\text{SrCu}_2(\text{BO}_3)_2$ as a function of magnetic field B . Using the standard Lanczos method, we solve a Shastry-Sutherland Hamiltonian with additional Dzyaloshinsky-Moriya (DM) terms which are crucial to explain different qualitative aspects of the ESR spectra. In particular, a nearest-neighbor DM interaction with a non-zero D_z component is required to explain the low frequency ESR lines for $B \parallel c$. This suggests that crystal symmetry is lowered at low temperatures due to a structural phase transition.

PACS numbers: 75.10.Jm, 75.40.Gb, 75.40.Mg, 75.45.+j, 75.50.Mm

I. INTRODUCTION

The spin liquids are states of matter that occur when quantum fluctuations are strong enough to avoid any type of magnetic ordering. This leads in general to a non-degenerate ground state and a finite gap for the spectrum of excitations. $\text{SrCu}_2(\text{BO}_3)_2$ is a quasi-two-dimensional spin system with a singlet dimer ground state¹. This compound is at present the only known realization of the Shastry-Sutherland model². In this model the effect of the quantum fluctuations is amplified by the geometrical frustration of the spin lattice. The low energy excitations of the ground state are local triplets whose "kinetic energy" is small compared to the repulsive triplet-triplet interaction. The application of a strong magnetic field induces a quantum phase transition in which the dimerized ground state starts to be populated with triplets. The magnetic field plays the role of a chemical potential for the triplet quasi-particles. In this scenario it is possible to study the competition between the "gaseous" triplet phase and the crystallization of triplets ("solid phase"). The crystallization of triplets gives rise to magnetization plateaus that have been observed in $\text{SrCu}_2(\text{BO}_3)_2$ ^{3,4}.

The anisotropic spin interactions are in general weak but they can have a strong effect on a highly frustrated system. In particular, as it was already established in Refs.^{5,6,7,8,9}, the inclusion of the nearest neighbor (nn) and next-nearest neighbor (nnn) Dzyaloshinsky-Moriya (DM) interactions is required to explain some qualitative features of the specific heat and electron spin resonance (ESR) experiments in $\text{SrCu}_2(\text{BO}_3)_2$. However, as it was noted recently by Cepas et al.^{5,6}, a lattice symmetry (reflection in the mirror plane containing the c -axis and one dimer followed by a rotation around the dimer bond) leads to a zero amplitude for the observed single-triplet ESR transitions for $B \parallel c$. In addition, a level anti-crossing between the ground state and the lowest triplet excitation is observed for $B \parallel c$ at 20 T. This level anti-crossing implies some mixing between two states with different magnetization M_z along the tetragonal c -axis, something that cannot be explained within the U(1) invariant models

(invariant under rotations around the c -axis) for which M_z is a good quantum number.

Recent experiments¹⁰ revealed additional quantitative and qualitative aspects of the ESR transitions. Besides the two non-degenerate one-triplet excitations, various types of multiple-triplet bound states forming singlets, triplets and quintuplets were identified. These measurements opened the possibility for a direct comparison between the observed family of magnetic excitations and the theoretical predictions based on the spin model proposed for $\text{SrCu}_2(\text{BO}_3)_2$ ¹¹. In addition, as it is shown in the present paper, they provide indirect information about the crystal symmetry at low temperatures and the role of the spin-lattice coupling as a function of the applied magnetic field B .

The considerable amplitude of the ESR absorption lines that according to the crystal symmetry are not expected to be observed poses a challenge for finding an adequate explanation. Cepas et al.⁶ proposed a mechanism based on a dynamically generated DM interaction induced by the spin-phonon coupling. However, they did not provide any comparison between a calculated ESR spectrum based on this mechanism and their experimental observation. In this paper we suggest that the crystal symmetry is lowered due to a structural phase transition that occurs in a low temperature region that has not yet been explored with X-rays. As a consequence, a non-zero c component of the nearest neighbor DM vector appears. In a previous paper,⁷ we showed that this component is required to reproduce the measured specific heat at low temperatures and high magnetic fields. Here, we show that the same component also explains the observed single-triplet ESR lines as well as other qualitative aspects of the ESR spectra as a function of $B \parallel c$ and $B \parallel a$.

II. MODEL HAMILTONIAN

To describe the present system, we consider the following Heisenberg Hamiltonian in a magnetic field on a

Shastry-Sutherland lattice²:

$$H_s = J \sum_{\langle i,j \rangle} S_i \cdot S_j + J^0 \sum_{\langle i,j \rangle^0} S_i \cdot S_j + g_B \sum_i S_i \cdot B + \sum_{\langle i,j \rangle} D \cdot (S_i - S_j) + \sum_{\langle i,j \rangle^0} D^0 \cdot (S_i - S_j): \quad (1)$$

Here, $\langle i,j \rangle$ and $\langle i,j \rangle^0$ indicate that i and j are nn and nnn, respectively. In addition to the Shastry-Sutherland Hamiltonian, H_s includes DM interactions to nn and nnn. The corresponding DM vectors are D and D^0 , respectively. The arrows indicate that bonds have a particular orientation as described in Ref.⁷. The quantization axis \hat{z} is parallel to the c -axis and \hat{x} to the a -axis. The nnn DM interaction has already been considered in previous papers¹¹ to explain the splitting between the two single-triplet excitations observed with ESR^{5,10}, far infra-red¹² and inelastic neutron scattering measurements¹³. The value of the DM interaction obtained from this splitting is: $D^0 = 2.1 \text{ K } \hat{z}$. According to the crystal symmetry¹⁴, only the xy component of D is non-zero and perpendicular to the corresponding dimer. However, as it is explained below, a non-zero z component of D is required to explain the specific heat and the ESR data for finite magnetic fields B .

For $D_z = 0$ and in two dimensions the relevant space group of H_s in Eq. (1) is $p4gm$, with a point group $4mm$ at $q = 0$ point in the Brillouin zone. However, the a - b plane in $\text{SrCu}_2(\text{BO}_3)_2$ containing dimers is slightly buckled and the (three dimensional) space group $P4_2m$ is more appropriate. Namely, the associated point group $42m$ includes the roto-inversion symmetry IC_4 (rotation through 90° around the c -axis followed by inversion I) which allows for a different orientation of the DM interaction with respect to the point group $4mm$, and thus results in lowering the ground state energy. In zero magnetic field H_s is moreover time-reversal invariant so that the point group at $q = 0$ should be enlarged to $G_M = 42m \oplus E$; g , where \oplus is the time-reversal operator and E is the identity operator.

III. ENERGY SPECTRUM

Numerical calculations were done using the standard Lanczos technique at zero temperature ($T = 0$) on a tilted square cluster of 20 sites. We start by analyzing the full energy spectrum for $q = 0$. Figs. 1a and 1b show the calculated energy spectra as a function of B \parallel c and B \parallel a , respectively. The vertical axis is in units of frequency to facilitate the comparison with the ESR experimental results by Nojima et al.¹⁰. With the exception of D_z^0 , the parameters of the model, $J = 74 \text{ K}$, $J^0 = 0.62J$, $D = (2.2 \text{ K}; 2.2 \text{ K}; 3.7 \text{ K})$, and $D^0 = (0; 0; 2.2 \text{ K})$, are the same as the ones used to fit the specific heat data for different values of the applied magnetic field⁷.

In both cases, there is a clear distinction between states that belong to the continuum in the thermodynamic limit

and those that will be called "localized" states. The bottom edge of the continuum appears around 1100 GHz above the ground state for $B = 0$. With increasing B this edge drops to 450 GHz at $B = 20 \text{ T}$ and then saturates as a function of B . Since the DM terms are small compared to J and J^0 , the localized states can be classified according to their approximate total spin quantum numbers, S and S_z , in the regime $B < 20 \text{ T}$. For $B < 6 \text{ T}$ there are at least four singlet and two triplet states split due to finite B and D_z^0 .

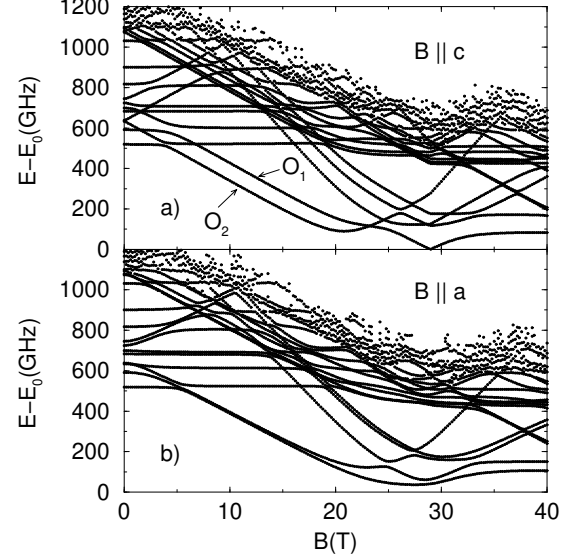


Figure 1: Energy spectrum relative to the ground state energy E_0 of the Hamiltonian H_s (Eq. (1)) calculated on a 20-site cluster with periodic boundary conditions for a) $B \parallel c$ and b) $B \parallel a$. The parameters of the model are: $J = 74 \text{ K}$, $J^0 = 0.62J$, $D = (2.2 \text{ K}; 2.2 \text{ K}; 3.7 \text{ K})$ and $D^0 = (0; 0; 2.2 \text{ K})$.

As it is expected from the Zeeman interaction, for $B \parallel c$ (Fig. 1a) the energy of the two $S_z = \pm 1$ triplet states (O_2 and O_1 in the notation of Ref.¹⁰) decreases linearly in the applied field. These two states are separated by an energy $\sim 90 \text{ GHz}$ and their position agrees well with experimental ESR lines observed in Refs.^{5,10}. A round $B_c = 20 \text{ T}$, the lower triplet state gets mixed with the singlet ground state producing a level anti-crossing that is a consequence of the finite values of D_x and D_y . For $D_z = 0$, only the lowest triplet state O_2 mixes with the singlet ground state. This is because the O_1 triplet state and the singlet ground state belong to different representations of the point group G_M . More precisely, a finite magnetic field breaks the π -invariance and reduces the symmetry from the full point group G_M to the (magnetic) subgroup $42m$ ¹⁵. The ground state and O_2 transform according to the irreducible representation A_1 of $42m$, while O_1 transforms according to B_2 . The main difference between these representations is in the fact that a roto-inversion with respect to the c -axis gives a sign $+1$ for the ground state and O_2 , while it gives -1 for O_1 .

The hybridization which is induced by a finite value of $D_z = 3.7$ K is too small to be observed with the ESR experiment in the absence of D_x and D_y terms. These findings are in agreement with the experimental data^{5,10}. For B ka the two triplet states are nearly degenerate except above $B = 20$ T. Again, in agreement with the experimental data^{5,10}, the two triplet states split around $B > 20$ T because of the different hybridization between each of them and the ground state. Note that the effect of this hybridization becomes significant when the energy difference between the triplets and the singlet ground state becomes comparable to DM interaction.

The agreement with the experiment extends even further. The level anti-crossing of triplet and singlet states around 646 GHz and 860 GHz for B ka is also reproduced (see Figs. 4b and 7 in Ref.¹⁰). Fig. 1b also shows a weak level anti-crossing of the O_1 $S_z = 1$ triplet state with the first singlet excitation located around 520 GHz. This effect seems to be too small to be experimentally observable. However, a much stronger level anti-crossing of the O_2 triplet with a singlet located around 600 GHz is observed at $B = 2.5$ T. Another strong level anti-crossing of the O_1 triplet with a singlet bound state is observed near $B = 4$ T and 800 GHz. Although the values of the magnetic fields of these anti-crossings are in good agreement with the experiment, the calculated frequencies deviate from the observed values. A comparison of the calculated ESR spectra for different cluster sizes suggests that this deviation is due to finite-size effects. For B kc, the O_1 triplet produces strong level anti-crossings for $B = 4.5$ T, $\nu = 600$ GHz and $B = 2.5$ T, $\nu = 800$ GHz. Experimentally, only the later crossing is clearly visible in Fig. 4a of Ref.¹⁰.

IV. SPIN STRUCTURE FACTOR

To make account of the frequency and the intensity of the ESR lines we need to compute the dynamical spin structure factor for $q = 0$,

$$S^*(\omega) = \frac{1}{Z} \text{Re} \int_0^{\omega} dt e^{i\omega t} \langle S^z(0) S^z(t) \rangle; \quad \omega = x, y \text{ or } z; \quad (2)$$

in the direction perpendicular to the applied magnetic field. The method that we used to compute $S^*(\omega)$ is described in Refs.^{16,17}. Fig. 2 shows the computed ESR spectrum as a function of frequency $\omega = \omega/2$ and the external magnetic field B along the c- and the a-axis. We use this frequency-field type of diagram to directly compare with the experimental data obtained by Nojiri et al.¹⁰. The best agreement with the experiment was found by normalizing the calculated intensity $S^*(\omega)$ in a way that its integral over all frequencies at a fixed magnetic field equals unity. In all figures presenting the calculated ESR spectrum such a normalized intensity is visualized by the height of the peaks (in arbitrary units). For B kc (see Fig. 2a) we obtain a finite spectral weight for the

two $S_z = 1$ triplet states O_2 and O_1 . The 90 GHz splitting between the O_2 and O_1 states is a consequence of the finite $D_z^0 = 2.2$ K. The level anti-crossing of the lowest O_2 triplet with the ground state near critical field $B_c = 20$ T is due to a finite value of intra-dimer DM interaction D_x, D_y , since these are the only interactions that break the rotational symmetry around the z-axis. These terms are also responsible for the level anti-crossings at $B = 4.5$ T, $\nu = 600$ GHz and $B = 2.5$ T, $\nu = 800$ GHz. Experimentally, only the later one is clearly visible in Fig. 4a of Ref.¹⁰. The overall effect of finite values of D_x, D_y can be clearly seen comparing Figs. 2a and 3a for which $D_x = D_y = 0$. For B kc there is no level anti-crossing neither with the singlet ground state, nor with excited singlets.

In principle, the D_x^0, D_y^0 terms could also contribute to level anti-crossing of O_1 and (or) O_2 states with the ground state. However, a closer analytical calculation shows, that these terms connect the ground state with a state, that consists of a product of two triplet states, the one with $S_z = 0$ and the other with $S_z = 1$, located on the two perpendicular dimers. This state is consequently orthogonal to O_1 and O_2 states. Therefore, one does not expect level anti-crossing in the first order in D_x^0, D_y^0 .

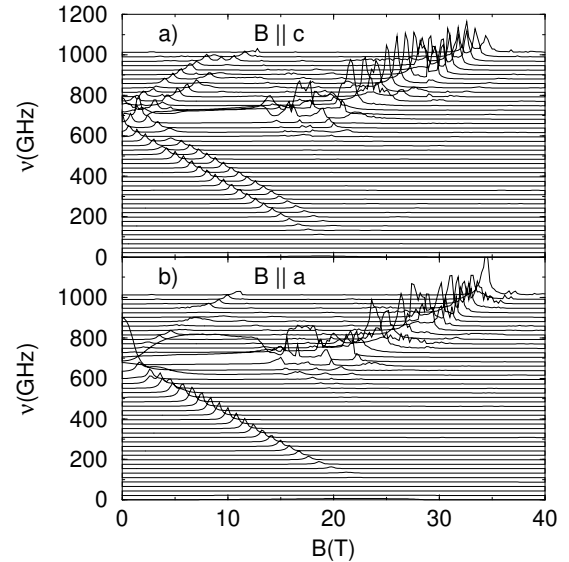


Figure 2: Spin structure factor a) $S^x(\omega)$ for B kc and b) $S^z(\omega)$ for B ka. Parameters of the model are: $J = 74$ K, $J^0 = 0.62J$, $D = (2.2 \text{ K}; 2.2 \text{ K}; 3.7 \text{ K})$ and $D^0 = (0; 0; 2.2 \text{ K})$. Note that the computed ESR spectrum is normalized as $\int d\omega S^*(\omega) = 1$ for any fixed B ($\omega = x, y, z$).

The finite intensities of O_1 and O_2 triplets for B kc are a consequence of a non-zero value of D_z which requires a lower crystal symmetry than the one observed with X-rays¹⁴. In Fig. 4 we show the calculated ESR spectra for $D_z = 0$. The O_1 and O_2 triplet lines are not observed for B kc while in B ka case, the lowest triplet excitations are clearly visible. Finite values of D_x, D_y or D_x^0, D_y^0

do not induce these transitions in the lowest order. The reason is that they mix $S_z = \pm 1$ states with the ground state. The non-zero D_z term is therefore the only term within the given Hamiltonian (1) that leads to O_1 and O_2 transitions for Bkc.

Comparing results of the model (1) with "optimally" chosen parameters (see Fig. 2) with the experiment in Ref.¹⁰ reveals a good agreement for the line positions, and in some cases even matching of level anti-crossings with singlet states. The main disagreement with the experiment is in line intensities. While on the one hand ESR measurements of Ref.¹⁰ show that for Bkc the O_1 line is nearly B-eld independent, O_2 line shows rather strong eld dependence: the intensity of the line increases with the applied magnetic eld. On the other hand, our numerical calculations in Fig. 2a show a nearly constant line intensities for both O_1 and O_2 lines.

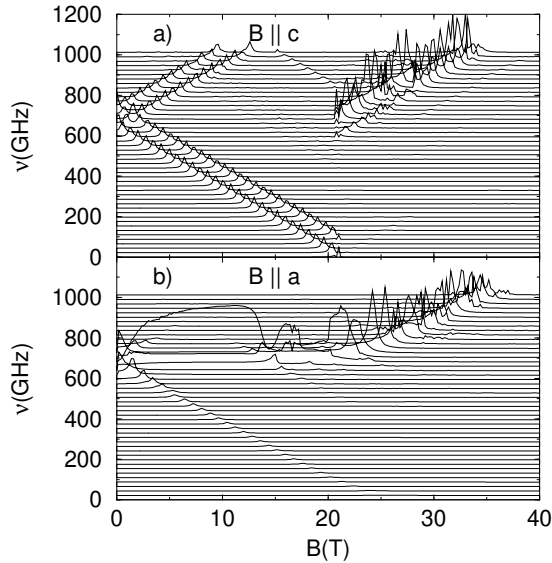


Figure 3: The same as in Fig. 2 except $D = (0; 0; 3; 7 \text{ K})$.

We focus now on the case Bka which is shown in Fig. 2b. The O_1 and O_2 triplets are nearly degenerate. A level anti-crossing with the ground state is well seen around $B \approx 20 \text{ T}$. The intensity of the $S_z = \pm 1$ lines is varying non monotonously with B . This non monotonous behavior could be due to a weak level anti-crossing with localized singlets at $\approx 600 \text{ GHz}$ observed in Fig. 1b. Pronounced level anti-crossings are obtained in the upper triplet branches with $S_z = \pm 1$. In contrast to the Bkc case, D_z is not the only term that leads to transitions between the ground state and the excited triplet states. In Figs. 3b and 4b we show S^z (!) for Bka and $D = (0; 0; 3; 7 \text{ K})$ and $D = (2; 2 \text{ K}; 2; 2 \text{ K}; 0)$, respectively. In both cases we see finite intensities of O_1 and O_2 triplets, however $D = (0; 0; 3; 7 \text{ K})$ leads to a smaller intensity than $D = (2; 2 \text{ K}; 2; 2 \text{ K}; 0)$. Note that even though intensities are presented in arbitrary units, the

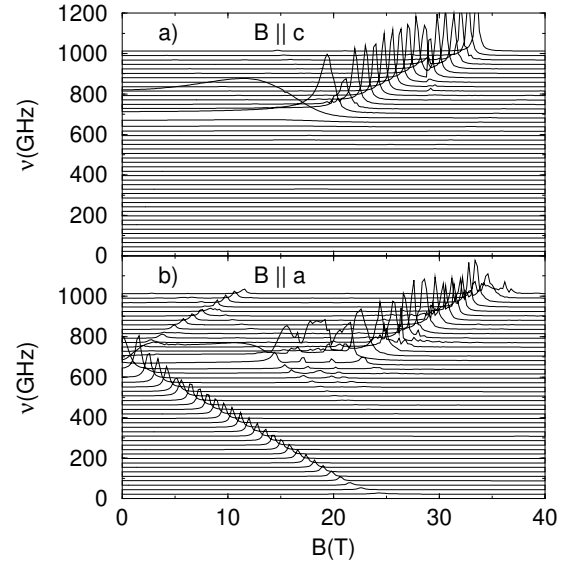


Figure 4: The same as in Fig. 2 except $D = (2; 2 \text{ K}; 2; 2 \text{ K}; 0)$.

scaling of intensities in all figures is identical to allow comparison.

V. CONCLUSIONS

In summary, the ESR spectra predicted by model (1) reproduce several aspects of the experimental data obtained by Nojima et al.¹⁰ for $\text{SrCu}_2(\text{BO}_3)_2$. In particular, for Bkc, the crystal symmetry breaking interaction D_z is the only term that leads to finite ESR intensities for O_1 and O_2 triplet states. We have tested other possible scenarios that could provide finite ESR intensities for the low-lying triplet excitations. One possibility is the introduction of an anisotropic gyromagnetic g-tensor (Zeeman term in Eq. (1)) with a different orientation for all 4 spins in the unit cell¹⁹. In order to get a finite ESR line for Bkc, the external eld coupled to the g-tensor would have to induce a staggered eld along the magnetic z-axis, such that each spin in a dimer would feel different eld orientation. However, due to the particular structure of the g-tensor, which is a consequence of the buckling of the ab planes in $\text{SrCu}_2(\text{BO}_3)_2$ ¹⁹, eld Bkc only induces staggered eld component along the x- and y-axis. A second possibility is the existence of a small finite angle between the crystallographic c-axis and the direction of the applied magnetic eld B due to an error in the orientation of the crystal. Taking into account that the off-diagonal component of the g-tensor is at most of the order of $g_{xy} \approx 0.05g_{xx} \approx 0.1$, we found at most no detectable signal for $\theta < 5^\circ$.

The inclusion of the DM interaction D_z provides the simplest way to explain some qualitative aspects of the ESR experiments for $\text{SrCu}_2(\text{BO}_3)_2$. This simple expla-

nation has very important experimental consequences. The existence of nonzero D_z suggests that the system should undergo a structural phase transition at low temperatures that lowers the crystal symmetry. In the new phase, the planes containing the c-axis and one dimer are no longer mirror planes. In addition, we also expect a strong spin-lattice coupling when the O_1 and O_2 triplet states get close to the singlet ground state. Such a coupling could contribute to the stabilization of the different plateaus that are observed in the magnetization vs. field experiments^{3,4}.

Acknowledgments

We wish to thank D. Aaron and A. Zorko for fruitful discussions as well as S. Zvyagin and H. Nojiri for their kind help with explaining the experimental setup. J.B., S.E.S. and I.S. acknowledge the financial support of Slovene MESS under contract P1-0044. This work was in part sponsored by the US DOE under contract W-7405-ENG-36.

-
- ¹ R.W. Smith and D.A. Keszler, *J. Solid State Chem.* **93**, 430 (1991).
 - ² B.S. Shastry and B. Sutherland, *Physica B* **108**, 1069 (1981).
 - ³ H. Kageyama, K. Yoshimura, R. Stem, N.V. M ushnikov, K. Onizuka, M. Kato, K. Kosuge, C.P. Slichter, T. Goto and Y. Ueda *Phys. Rev. Lett.* **82**, 3168 (1999).
 - ⁴ K. Onizuka, H. Kageyama, Y. Narumi, K. Kondo, Y. Ueda and T. Goto, *J. Phys. Soc. Jpn.* **69**, 1016 (2000).
 - ⁵ O. Cepas, K. Kakurai, L.P. Regnault, T. Ziman, J.P. Boucher, N. Aso, M. Nishi, H. Kageyama and Y. Ueda, *Phys. Rev. Lett.* **87**, 167205 (2001).
 - ⁶ O. Cepas, T. Sakai and T. Ziman, *Prog. Theor. Phys. Suppl.* **145**, 43 (2002).
 - ⁷ G.A. Jorge, R. Stem, M. Jaime, N. Harrison, J. Bonca, S.ElShawish, C.D. Batista, H.A. Dabkowska and B.D. Gaulin, cond-mat/0309534.
 - ⁸ A. Zorko, D. Aaron, H. Kageyama and A. Lappas, cond-mat/0310178.
 - ⁹ A. Zorko, D. Aaron, H. van Tol, L.C. Brunel and H. Kageyama, cond-mat/0311079.
 - ¹⁰ H. Nojiri, H. Kageyama, Y. Ueda and M. Motokawa, *J. Phys. Soc. Jpn.* **72**, 3243 (2003).
 - ¹¹ S. Miyahara and K. Ueda, *J. Phys.: Condens. Matter* **15**, R 327 (2003).
 - ¹² T. Roem, U. Nagel, E. Lippmaa, H. Kageyama, K. Onizuka and Y. Ueda, *Phys. Rev. B* **61**, 14342 (2000).
 - ¹³ H. Kageyama, M. Nishi, N. Aso, K. Onizuka, T. Yoshimura, K. Nukui, K. Kodama, K. Kakurai and Y. Ueda, *Phys. Rev. Lett.* **84**, 5876 (2000).
 - ¹⁴ K. Sparta, G. J. Redhammer, P. Roussel, G. Heger, G. Roth, P. Lemmens, A. Ionescu, M. Grove, G. Guntherodt, F. Huning, H. Lueken, H. Kageyama, K. Onizuka and Y. Ueda, *Eur. Phys. J. B* **19**, 507 (2001).
 - ¹⁵ see, e.g., M. Hamermesh, *Group Theory and Its Application to Physical Problems* (Addison-Wesley, Reading Massachusetts, 1962).
 - ¹⁶ E.R. Gagliano and C.A. Balseiro, *Phys. Rev. Lett.* **59**, 2999 (1987).
 - ¹⁷ J. Jaklic and P. Prelovsek, *Adv. Phys.* **49**, 1 (2000).
 - ¹⁸ S. Zherlitsyn, S. Schmidt, B. Wolf, H. Schwenk, B. Luthi, H. Kageyama, K. Onizuka, Y. Ueda and K. Ueda, *Phys. Rev. B* **62**, R 6097 (2000).
 - ¹⁹ K. Kodama, S. Miyahara, M. Takigawa, M. Horvatic, C. Berthier, F. Mila, H. Kageyama and Y. Ueda, cond-mat/0404482.